CRACK GROWTH ANALYSIS IN REINFORCED CONCRETE USING BEM

By A. L. Saleh[1] and M. H. Aliabadi[2]

ABSTRACT: A boundary-element formulation for modeling the nonlinear behavior of reinforced concrete is presented. The influence of reinforcements on the concrete is considered as a distribution of forces over the region of attachment. The solution for the attachment forces is obtained from the condition that the deformations of the concrete and the reinforcement under the action of the external loading are compatible. The yielding of reinforcement is considered when the total force at any section of the reinforcement is greater than the yielding force and is assumed to be broken when the strain reaches the maximum strain. The fracture of concrete is simulated using the fictitious crack model in which the fracture zone is replaced by closing forces acting on both crack surfaces. In using the boundary-element method to simulate cracks, the crack path is not known in advance because it can be calculated during the iteration process, and then the need of remeshing becomes obsolete. The numerical results obtained are compared to the finite-element method analysis and experimental results.

INTRODUCTION

Reinforced concrete is a composite material in which steel reinforcements are provided in the region of tension. In a typical situation, concrete is cracked and transmits mainly compressive stresses, while reinforcement carries the tensile stresses. Since cracking has a major influence on the structural performance and because of the practical importance of this problem, much research has been devoted to its solution. Recent developments have been strongly influenced by the application of the finite-element method (FEM) to the analysis of cracks in the reinforced-concrete structures. The FEM in conjunction with constitutive relationships permits the numerical simulation of the nonlinear stress-strain behavior of the materials. Concrete cracking is perhaps one of the major contributing factors to the nonlinear behavior of the material. Generally, numerical models for analyzing crack growth in concrete may be distinguished in two categories: (1) The discrete crack model; and (2) the smeared crack model.

The application of the boundary-element method (BEM) to simulate crack growth in reinforced concrete is a new subject. Therefore, the aim of this paper is to fill this gap and extend the work in Saleh and Aliabadi (1995) to include steel reinforcement in the model. The fictitious crack model (FCM) is used for the cracking of concrete and is bonded by stiffener to represent the reinforcement. The dual boundary-element method (DBEM) has been employed in the analysis. The result obtained is compared to the FEM analysis and experimental result.

The advantage of the method proposed in this paper and others lies mainly in the simple modeling requirement to follow the crack growth in the reinforced-concrete structures.

CRACKING OF CONCRETE

The tensile cracking of concrete creates physical discontinuities. To model this problem, a fictitious crack approach has been employed. The FCM is a theory applicable to numerical calculation of crack propagation in a concrete structure or a structure of similar materials having a low ultimate tensile strength. The model is based on the following assumptions:

1. The fracture zone starts to develop at one point when the maximum principal stress reaches the maximum tensile stress.
2. The fracture zone develops perpendicular to the maximum principal stress.
3. The material in the fracture zone is partly destroyed but is still able to transfer stress. The stress is dependent on the crack opening displacement.
4. The material properties outside the fracture zone are assumed to be linear elastic and given by σ-ε relationship.

In the model the fracture zone is replaced by closing forces (or cohesive forces) acting on both crack surfaces and the intensity of these forces are dependent on the crack opening displacement [Fig. 1(a)]. The relationship between stress and crack opening displacement is considered to be straight line (SL) and bilinear line (BL) as shown in Fig. 1(b). When the stress at the fictitious crack tip exceeds the maximum tensile strength of the concrete, the fictitious crack will propagate perpendicular to the maximum principal stress. The fictitious crack will become an open crack (traction-free) if the crack opening displacement Δu^{cr} is greater than the critical crack opening displacement Δu_c^{cr}.

DBEM

In this paper, the DBEM is extended to model the cracking of reinforced concrete. The DBEM is shown to be computationally efficient in simulating crack propagation especially when dealing with the nonlinearity behavior in concrete. The dual equations, on which the DBEM is based, are the displacement and the traction boundary integral equations. The boundary integral representation of the displacement components u_j can be written in terms of boundary point as

$$c_{ij}(\mathbf{x}')u_j(\mathbf{x}') + \oint_{\Gamma-\Gamma_{cr}} T_{ij}(\mathbf{x}', \mathbf{x})u_j(\mathbf{x})\, d\Gamma(\mathbf{x}) + \oint_{\Gamma_{cr}} T_{ij}(\mathbf{x}', \mathbf{x})u_j^{cr}(\mathbf{x})\, d\Gamma_{cr}(\mathbf{x}) - \int_{\Gamma_{cr}} U_{ij}(\mathbf{x}', \mathbf{x})t_j^{cr}(\mathbf{x})\, d\Gamma_{cr}(\mathbf{x}) = \int_{\Gamma-\Gamma_{cr}} U_{ij}(\mathbf{x}', \mathbf{x})t_j(\mathbf{x})\, d\Gamma(\mathbf{x}) \tag{1}$$

assuming continuity of the displacement at $\mathbf{x}'$, the collocation point. The coefficient $c_{ij}(\mathbf{x}')$ is given by $\delta_{ij}/2$ for smooth boundary at the point $\mathbf{x}'$ (δ_{ij} is the Kronecker delta), and $\oint$ is the Cauchy principal value integral. The functions $T_{ij}(\mathbf{x}', \mathbf{x})$

[1]Lect., Facu. of Civ. Engrg., Universiti Teknologi Malaysia, Locked Bag 791, 80990 Johor Bahru, Johor, Malaysia.
[2]Dir. of Computational Mech., Dept. of Engrg., Queen Mary and Westfield Coll., Univ. of London, Mile End, London E1 4NS, England.

Note. Associate Editor: Sunil Saigal. Discussion open until February 1, 1999. To extend the closing date one month, a written request must be filed with the ASCE Manager of Journals. The manuscript for this paper was submitted for review and possible publication on March 14, 1996. This paper is part of the ***Journal of Engineering Mechanics***, Vol. 124, No. 9, September, 1998. ©ASCE, ISSN 0733-9399/98/0009-0949–0958/ $8.00 + $.50 per page. Paper No. 12879.

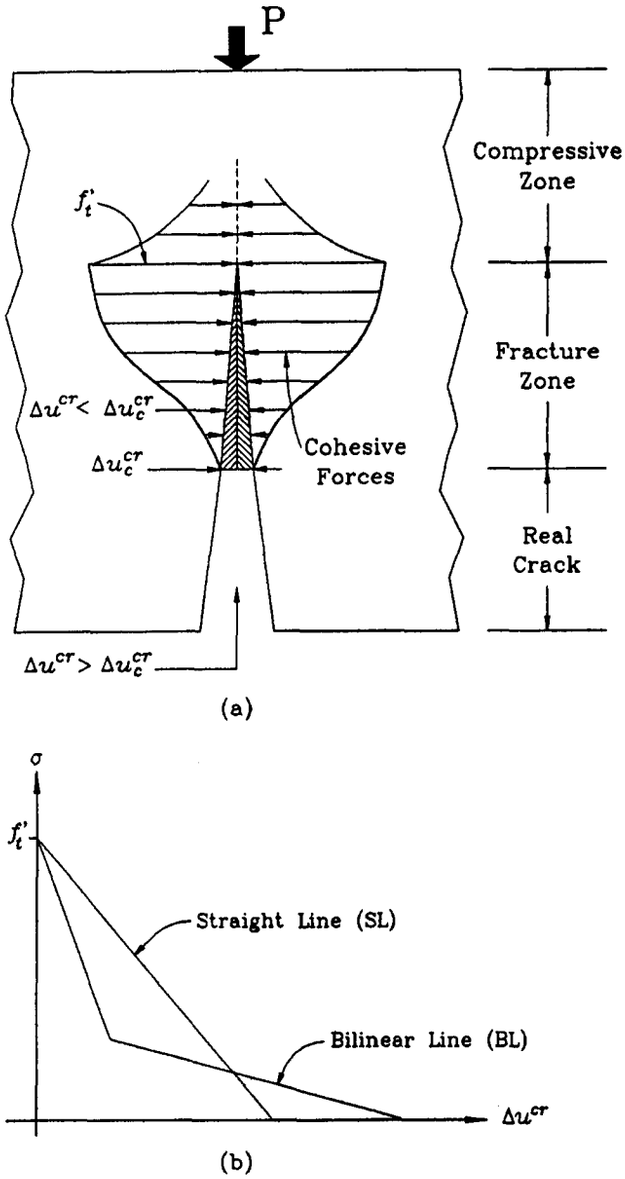

FIG. 1. FCM: (a) Fracture Zone Is Replaced by Cohesive Forces; (b) Relationship of σ-Δu^{cr} Curve

and $U_{ij}(\mathbf{x}', \mathbf{x})$ represent the Kelvin traction and displacement fundamental solutions, respectively. At a boundary point $\mathbf{x}$, $u_j^{cr}(\mathbf{x})$ and $t_j^{cr}(\mathbf{x})$ are the displacement and distributed cohesive forces, respectively, on one of the crack surfaces Γ_{cr}.

The boundary integral representation of the traction components t_j can be obtained from $t_j = \sigma_{ij} n_i$, where σ_{ij} are the stress components obtained by differentiating equation (1) followed by application of Hooke's law, and n_i denotes the ith component of the unit outward normal to the boundary. For a point on a smooth boundary, t_j can be written as

$$\frac{1}{2} t_j(\mathbf{x}') + n_i(\mathbf{x}') \oint_{\Gamma - \Gamma_{cr}} S_{kij}(\mathbf{x}', \mathbf{x}) u_k(\mathbf{x})\, d\Gamma(\mathbf{x})$$

$$+ n_i(\mathbf{x}') \oint_{\Gamma_{cr}} S_{kij}(\mathbf{x}', \mathbf{x}) u_k^{cr}(\mathbf{x})\, d\Gamma_{cr}(\mathbf{x})$$

$$- n_i(\mathbf{x}') \int_{\Gamma_{cr}} D_{kij}(\mathbf{x}', \mathbf{x}) t_k^{cr}(\mathbf{x})\, d\Gamma_{cr}(\mathbf{x})$$

$$= n_i(\mathbf{x}') \oint_{\Gamma - \Gamma_{cr}} D_{kij}(\mathbf{x}', \mathbf{x}) t_k(\mathbf{x})\, d\Gamma(\mathbf{x}) \tag{2}$$

where $S_{kij}(\mathbf{x}', \mathbf{x})$ and $D_{kij}(\mathbf{x}', \mathbf{x})$ = linear combinations of derivatives of $T_{ij}(\mathbf{x}', \mathbf{x})$ and $U_{ij}(\mathbf{x}', \mathbf{x})$, respectively. $\oint$ denotes the Hadamad principal value integral. The functions $u_k^{cr}(\mathbf{x})$ and $t_k^{cr}(\mathbf{x})$ are the displacement and distributed cohesive forces, respectively, at the other crack surfaces Γ_{cr}. For a traction-free crack, $t_j^{cr} = t_k^{cr} = 0$. Eqs. (1) and (2) constitute the basis of the DBEM and can be expressed in the matrix form as

$$[A \ [H_{cr}] \ [G_{cr}]] \begin{Bmatrix} X \\ \{u_{cr}\} \\ \{t_{cr}\} \end{Bmatrix} = \{F\} \tag{3}$$

in which A = coefficient corresponding to the vector X containing unknowns u and t; and $\{F\}$ contains the known values of u and t on the boundary nodes other than crack boundary. $[H_{cr}]$ and $G_{cr}]$ are coefficients corresponding to the nodes on the crack boundary.

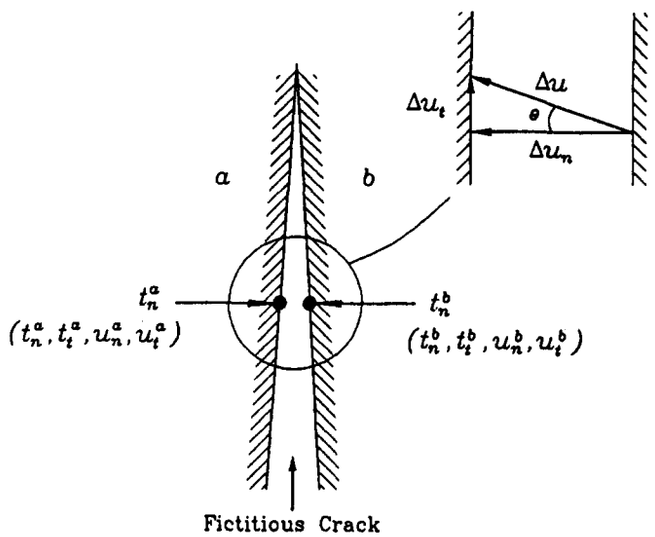

FIG. 2. Unknown Parameters at Fictitious Crack Surfaces *a* and *b*

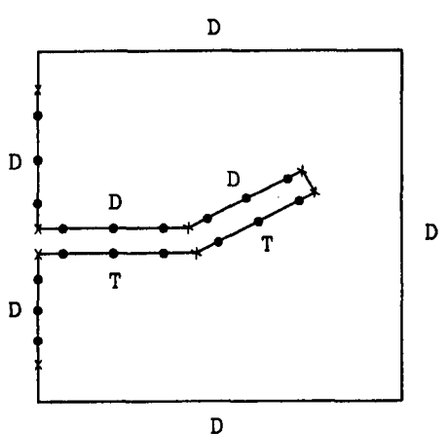

FIG. 3. Crack Modeling Strategy

BOUNDARY CONDITION FOR FCM

The cohesive forces on the fictitious crack surfaces, i.e., the fracture zone, can be derived by the relationship between traction and crack opening displacement in the local coordinate system (n, t). The linear (SL) softening constitutive law [see Fig. 1(b)] can be written as

$$t_n^{cr} = f_t' \left(1 - \frac{\Delta u_n^{cr}}{\Delta u_c^{cr}}\right), \quad t_{nt}^{cr} = 0 \tag{4}$$

where $\Delta u_n^{cr} = u_n^b - u_n^a$ = displacement discontinuity normal to the crack in which u_n^a = displacement at one of the crack surfaces; and u_n^b = displacement at the opposite crack surfaces as shown in Fig. 2. Δu_c^{cr} and f_t' are the material parameters. At the interface of the fracture zone, to maintain the equilibrium, the following conditions are enforced:

$$u_n^a = u_n^b; \quad t_n^a = -t_n^b; \quad t_t^a = -t_t^b \tag{5a-c}$$

The combination of boundary integral equations, [(1) and (2)] and the fictitious crack boundary conditions [(3) and (4)] can be expressed in the matrix form as

$$\begin{bmatrix} A & [H_{cr}] & [G_{cr}] \\ 0 & [C_{cr}] & [D_{cr}] \end{bmatrix} \begin{Bmatrix} X \\ \{u_{cr}\} \\ \{t_{cr}\} \end{Bmatrix} = \begin{Bmatrix} F \\ \{S_{cr}\} \end{Bmatrix} \tag{6}$$

where $[C_{cr}]$ and $[D_{cr}]$ = fictitious crack boundary conditions corresponding to the vectors $\{u_{cr}\}$ and $\{t_{cr}\}$, respectively; and the vector $\{S_{cr}\}$ contains the material parameters. In all cases, subscript cr represents the fictitious crack boundary. For the linear relation of σ-Δu_n^{cr}, matrices $[C_{cr}]$ and $[D_{cr}]$ contain 4 × 4 submatrices given by

$$[C_{cr}] = \begin{bmatrix} -\dfrac{f_t'}{\Delta u_c^{cr}} & 0 & \dfrac{f_t'}{\Delta u_c^{cr}} & 0 \\ 0 & -1 & 0 & 1 \\ 0 & 0 & 0 & 0 \\ 0 & 0 & 0 & 0 \end{bmatrix} \tag{7a}$$

$$[D_{cr}] = \begin{bmatrix} 1 & 0 & 0 & 0 \\ 0 & 0 & 0 & 0 \\ 1 & 0 & 1 & 0 \\ 0 & 1 & 0 & 1 \end{bmatrix} \tag{7b}$$

and vectors $\{u_{cr}\}$, $\{t_{cr}\}$, and $\{S_{cr}\}$ are given by

$$\{u_{cr}\} = [N] \begin{Bmatrix} u_x^a \\ u_y^a \\ u_x^b \\ u_y^b \end{Bmatrix}; \quad \{t_{cr}\} = [N] \begin{Bmatrix} t_x^a \\ t_y^a \\ t_x^b \\ t_y^b \end{Bmatrix}; \quad \{S_{cr}\} = \begin{Bmatrix} f_t' \\ 0 \\ 0 \\ 0 \end{Bmatrix} \tag{8a-c}$$

where $[N]$ = transformation matrix from global to the local

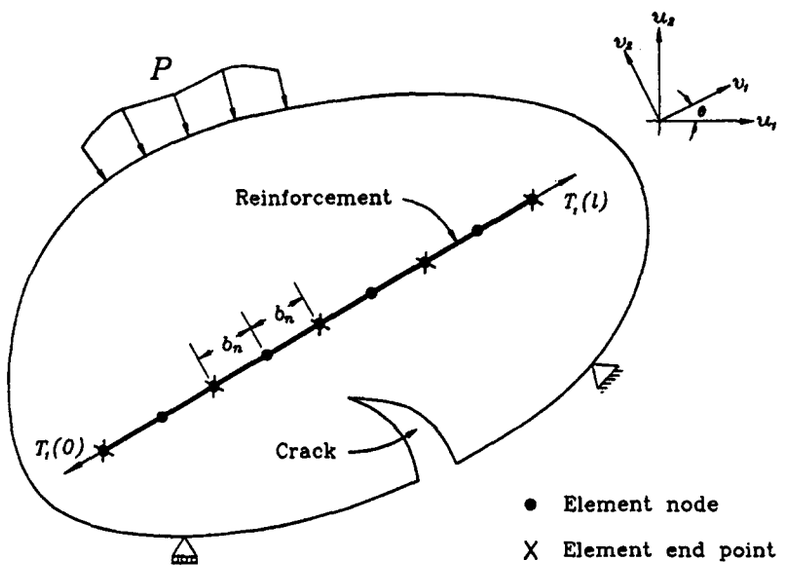

(a)

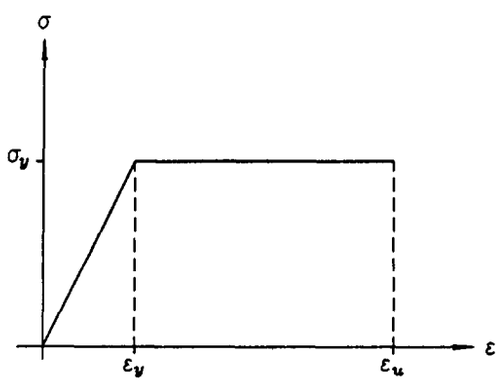

(b)

FIG. 4. Reinforced-Concrete Configuration: (a) Steel Reinforcement Node Separated by Equal Interval b_n; (b) Stress-Strain Curve for Steel Is Assumed to Be Linear Perfectly Plastic

reference system, varying node by node on the fictitious crack surface.

The cracked boundaries are modeled with discontinuous quadratic elements (see Fig. 3). This is due to efficiency and to keep the simplicity of the standard boundary elements. Continuous quadratic elements are used along the remaining boundary of the body, except at the intersection between a crack and an edge, where discontinuous elements are required on the edge to avoid a common node at the intersection.

MODELING OF REINFORCEMENTS

In general, three approaches are used to take into account the effect of steel reinforcement in the calculation of stresses in the reinforced-concrete members: (1) smear model; (2) embedded model; and (3) discrete model.

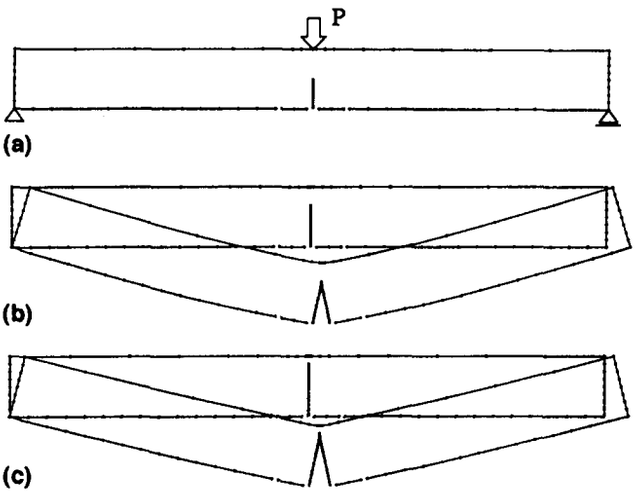

FIG. 5. (a) Boundary-Element Mesh; Deformed Shape for: (b) Iteration 4; (c) Iteration 8

In the present study, the embedded model is coupled with the BEM to study the effect of the reinforcement in the simulation of crack propagation of the reinforced-concrete beam. When using this model, the following assumptions are made:

1. The bond between concrete and reinforcement is assumed to be perfect.
2. The stiffness contribution of the reinforcement is only in the longitudinal direction.
3. Reinforcement is straight and has a constant cross-sectional area.
4. Dowel action, shear transfer, and aggregate interlock are not taken into account.

Using the embedded model, the influence of reinforcements on the concrete can be considered as a distribution of forces over the region of attachment, which for balance configurations may be considered as body forces. In this case, the behavior of the concrete may be described using the theory of generalized plane stress, and the theoretical modeling of the reinforcement is a problem in terms of the unknown attachment force distribution. The solution for the attachment forces is obtained from the condition that the deformation of the concrete and the reinforcement under the action of the external loading are compatible.

Development of Numerical Model

Consider a cracked reinforced-concrete configuration in Fig. 4(a). In addition to the plain concrete, a number of reinforcements are bonded to the concrete over the loci L_n (n = 1, 2, . . . , N^{st}, where N^{st} is the number of reinforcement). The reinforcement is subdivided into a continuous quadratic isoparametric element that consists of three nodes with an equal interval b_n. Each reinforcement exerts a line distribution of force (per unit arc length) $f_j^n(\mathbf{X})$ (j = 1, 2; n = 1, 2, . . . , N^{st})

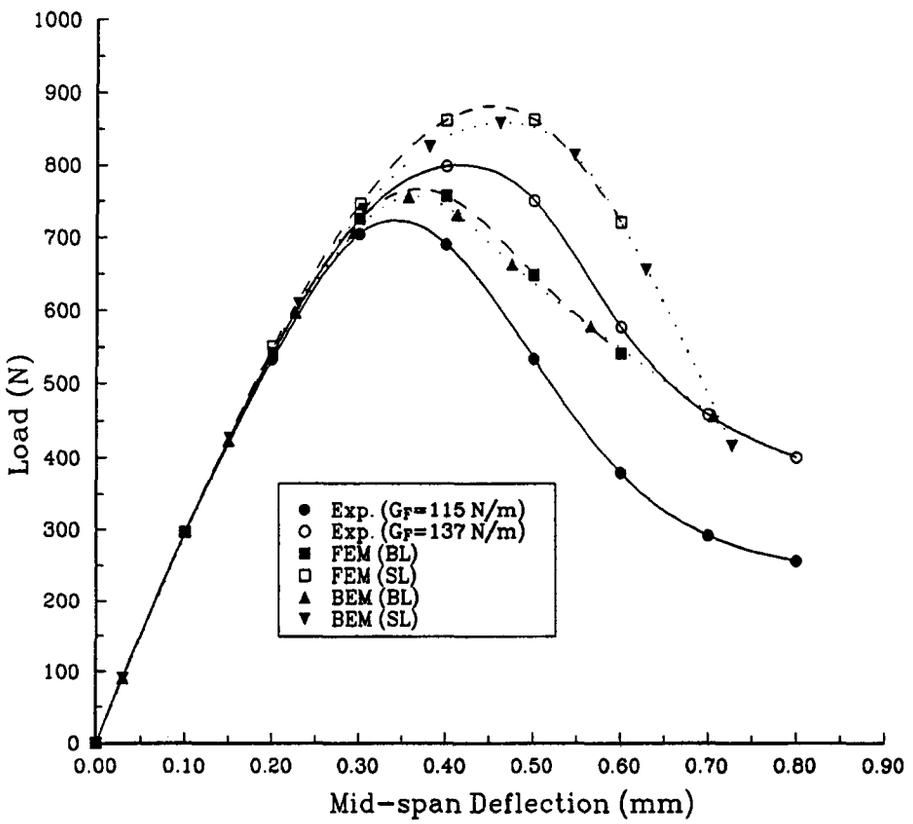

FIG. 6. Load-Deflection Curves Obtained by BEM Analysis, FEM Analysis, and Experimental Results

on the corresponding locus L_n in the concrete, and it experiences an equal and opposite reaction force $-f_j^n(\mathbf{X})$ along its length. The condition that the displacements of the concrete $u_j(\mathbf{X})$ and the nth reinforcement $u_j^n(\mathbf{X})$ are compatible with the shear coefficient of the bond between concrete and reinforcement Φ^n and is given in term of f_j^n by

$$[u_j^n(\mathbf{X}') - u_j^n(\mathbf{X}_0)] - [u_j(\mathbf{X}') - u_j(\mathbf{X}_0)] = \Phi^n[f_j^n(\mathbf{X}') - f_j^n(\mathbf{X}_0)] \tag{9}$$

where $\mathbf{X}_0$ and $\mathbf{X}'$ = distinct points on the nth reinforcement locus L_n. For a perfect bond, Φ^n is equal to zero.

The reaction forces of the reinforcement $f_j^n(\mathbf{X})$ can be included in the displacement boundary integral equation [(1)] as the body forces confined to a straight line instead of the domain and is given by

$$c_{ij}(\mathbf{x}')u_j(\mathbf{x}') + \oint_{\Gamma-\Gamma_{cr}} T_{ij}(\mathbf{x}', \mathbf{x})u_j(\mathbf{x})\, d\Gamma(\mathbf{x}) + \oint_{\Gamma_{cr}} T_{ij}(\mathbf{x}', \mathbf{x})u_j^{cr}(\mathbf{x})\, d\Gamma_{cr}(\mathbf{x}) - \int_{\Gamma_{cr}} U_{ij}(\mathbf{x}', \mathbf{x})t_j^{cr}(\mathbf{x})\, d\Gamma_{cr}(\mathbf{x}) - \sum_{n=1}^{N^{st}} \int_{L_n} U_{ij}(\mathbf{x}', \mathbf{X})f_j^n(\mathbf{X})\, dL_n(\mathbf{X}) = \int_{\Gamma-\Gamma_{cr}} U_{ij}(\mathbf{x}', \mathbf{x})t_j(\mathbf{x})\, d\Gamma(\mathbf{x}) \tag{10}$$

and in the traction boundary integral equation [(2)] as

$$\frac{1}{2}t_j(\mathbf{x}') + n_i(\mathbf{x}') \oint_{\Gamma-\Gamma_{cr}} S_{kij}(\mathbf{x}', \mathbf{x})u_k(\mathbf{x})\, d\Gamma(\mathbf{x}) + n_i(\mathbf{x}') \oint_{\Gamma_{cr}} S_{kij}(\mathbf{x}', \mathbf{x})u_k^{cr}(\mathbf{x})\, d\Gamma_{cr}(\mathbf{x}) - n_i(\mathbf{x}') \oint_{\Gamma_{cr}} D_{kij}(\mathbf{x}', \mathbf{x})t_k^{cr}(\mathbf{x})\, d\Gamma_{cr}(\mathbf{x}) - n_i(\mathbf{x}') \sum_{n=1}^{N^{st}} \int_{L_n} D_{ijk}(\mathbf{x}', \mathbf{X})f_k^n(\mathbf{X})\, dL_n(\mathbf{X}) = n_i(\mathbf{x}') \oint_{\Gamma-\Gamma_{cr}} D_{kij}(\mathbf{x}', \mathbf{x})t_k(\mathbf{x})\, d\Gamma(\mathbf{x}) \tag{11}$$

Combining (9) with (10) and (11) gives the compatibility equation for points $\mathbf{X}_0$ and $\mathbf{X}'$ on the nth reinforcement locus as

$$[u_j^n(\mathbf{X}') - u_j^n(\mathbf{X}_0)] + \oint_{\Gamma-\Gamma_{cr}} \Delta T_{ij}u_j(\mathbf{x})\, d\Gamma(\mathbf{x}) + \oint_{\Gamma-\Gamma_{cr}} \Delta T_{ij}u_j^{cr}(\mathbf{x})\, d\Gamma_{cr}(\mathbf{x}) - \int_{\Gamma_{cr}} \Delta U_{ij}t_j^{cr}(\mathbf{x})\, d\Gamma_{cr}(\mathbf{x}) - n_i(\mathbf{X}) \oint_{\Gamma} \Delta S_{kij}u_k(\mathbf{x})\, d\Gamma(\mathbf{x}) - n_i(\mathbf{X}) \oint_{\Gamma_{cr}} \Delta D_{kij}t_k^{cr}(\mathbf{x})\, d\Gamma_{cr}(\mathbf{x}) - \sum_{n=1}^{N^{st}} \int_{L_n} U_{ij}(\mathbf{X}' - \mathbf{X}_0)f_j^n(\mathbf{X})\, dL_n(\mathbf{X}) = \int_{\Gamma-\Gamma_{cr}} \Delta U_{ij}t_j(\mathbf{x})\, d\Gamma(\mathbf{x}) + n_i(\mathbf{X}) \oint_{\Gamma-\Gamma_{cr}} \Delta D_{kij}t_k(\mathbf{x})\, d\Gamma(\mathbf{x}) \tag{12}$$

where $\Phi^n = 0$ is assumed and

$$\Delta T_{ij} = T_{ij}(\mathbf{X}', \mathbf{x}) - T_{ij}(\mathbf{X}_0, \mathbf{x}) \tag{13a}$$

$$\Delta U_{ij} = U_{ij}(\mathbf{X}', \mathbf{x}) - U_{ij}(\mathbf{X}_0, \mathbf{x}) \tag{13b}$$

$$\Delta S_{kij} = S_{kij}(\mathbf{X}', \mathbf{x}) - S_{kij}(\mathbf{X}_0, \mathbf{x}) \tag{13c}$$

$$\Delta D_{kij} = D_{kij}(\mathbf{X}', \mathbf{x}) - D_{kij}(\mathbf{X}_0, \mathbf{x}) \tag{13d}$$

The displacements u_j^n of the nth reinforcement in (12) can be expressed in terms of an arc length parameter x measured in the longitudinal direction from one end. Therefore, the relative displacement of the reinforcement due to a body force distribution $-f_j(x)$ per unit length $(0 < x \leq l)$ are given by

$$u_j(x) - u_j(0) = [N][v_j(x) - v_j(0)] \quad \text{for} \quad j = 1, 2 \tag{14}$$

where $[N]$ represents the transformation matrix from global to local coordinate system. The displacements v_j of the reinforcement along the longitudinal directions are given as

$$[v_1(x) - v_1(0)] = \frac{1}{A_sE_s}\left\{xT_1(0) + \int_0^x (x - \xi)f_1(\xi)\, d\xi\right\} \tag{15}$$

and along the transverse direction as

$$[v_2(x) - v_2(0)] = \frac{1}{A_sG_s}\left\{xT_2(0) + \int_0^x (x - \xi)f_2(\xi)\, d\xi\right\} - \frac{1}{R_s}\left\{\frac{1}{2}x^2M(0) + \frac{1}{6}x^3T_2(0) + \int_0^x \frac{1}{6}(x - \xi)^3f_2(\xi)\, d\xi\right\} - x\beta(0) \tag{16}$$

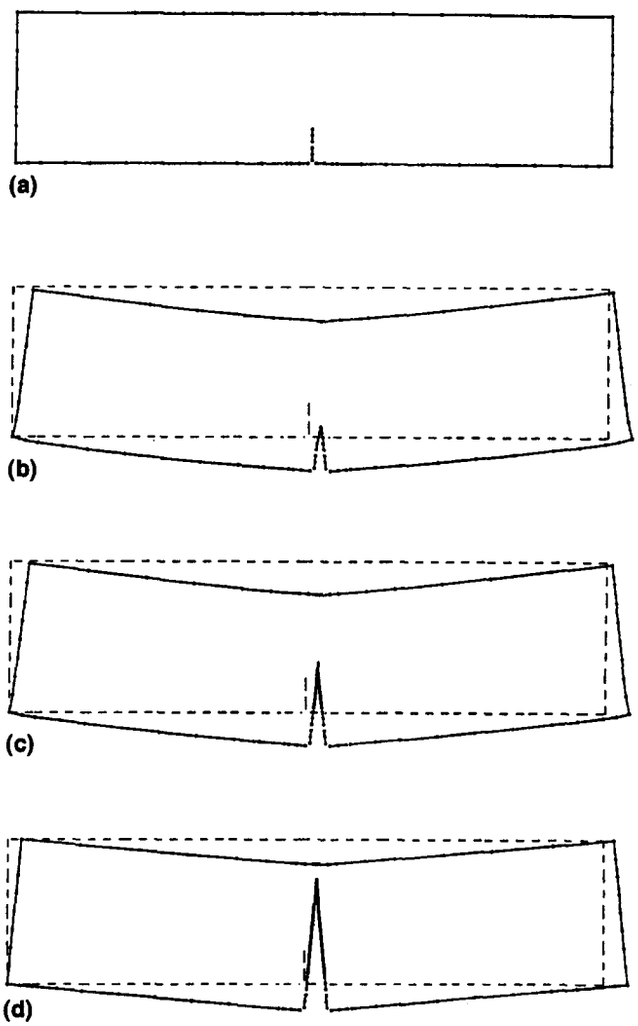

FIG. 7. (a) Boundary-Element Mesh; Deformed Shapes for: (b) Iteration 4; (c) Iteration 8; (d) Final Load

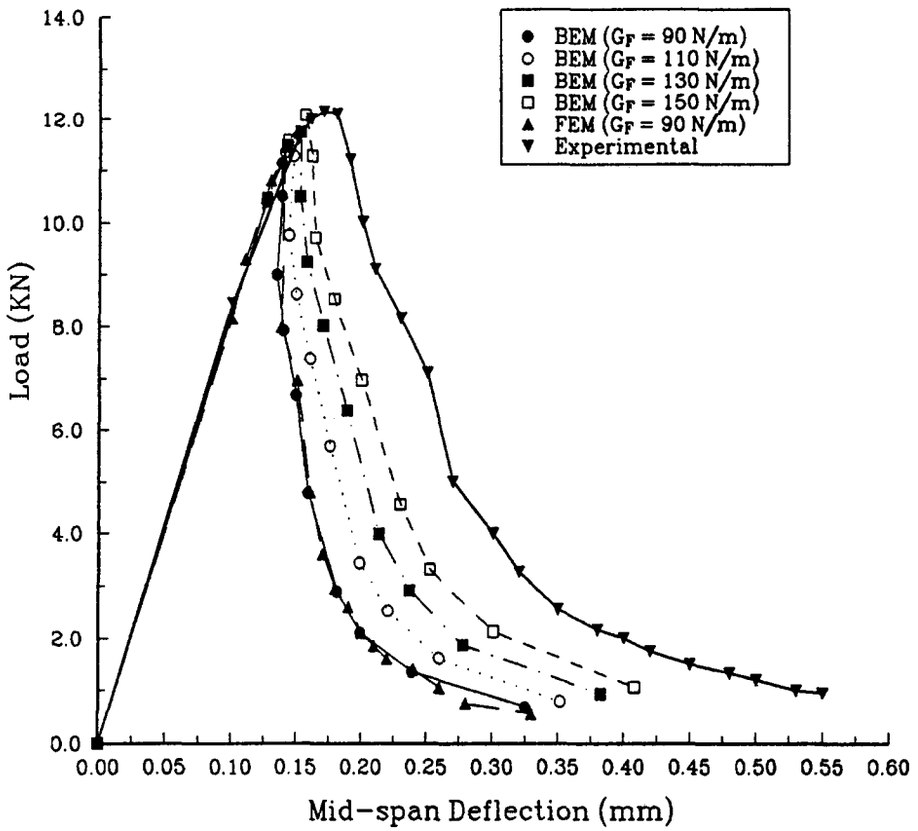

FIG. 8. Load-Deflection Curves for Plain Concrete Beam with Various G_F

where A_s, E_s, G_s, and R_s = material properties that represent the cross-sectional area, Young's modulus, shear modulus, and transverse flexural rigidity of the reinforcements, respectively. $T_1(x)$, $T_2(x)$, and $M(x)$ representing the internal forces and moment acting over the reinforcement cross section and $\beta(0)$ denoting the partial derivative $\partial v_1/\partial y$ evaluated at the end $x = 0$ to take account for any difference in the rigid body rotations of the reinforcement and the concrete.

Additional equations are the equilibrium state under the action of the body forces $-f_j(x)$ and the end loads $T_1(0)$, $T_1(l)$; $T_2(0)$, $T_2(l)$; and $M(0)$, $M(l)$. They can be expressed as

$$\int_0^l f_j(x)\,dx = T_j(l) - T_j(0) \quad \text{for} \quad j = 1, 2 \tag{17a}$$

$$\int_0^l (l - x) f_2(x)\,dx = M(l) - M(0) - lT_2(0) \tag{17b}$$

The end loads in (17) correspond to the boundary conditions for the reinforcement. Setting all six values to zero will represent a reinforcement with free ends. Alternatively, the values may be chosen to specify a given state of stress or strain at the ends.

YIELDING OF REINFORCEMENT

The reinforcements are assumed to behave linearly up to the yield stress σ_Y and then as a perfectly plastic material as shown in the stress-strain curve in Fig. 4(b). After yielding, the force in the reinforcement is set to the yielding force $F_y = \sigma_Y A_s$ until the strain reaches the maximum strain ε_{su}, where the reinforcement is broken. The total force at any node in the reinforcement F_n is determined from the end load $T_1(0)$ and the summation of forces (per unit arc length) f_j multiplied by the node interval b_n as

$$F_n = T_1(0) + b_n \sum_{j=n}^{N} f_j \tag{18}$$

The total force in (18) is compared with the yielding force F_y. If the force is greater than the yielding force, all the affected nodes ($j = n, \ldots, N$) are set to a value in such a way that the summation of forces per unit arc length at that particular node is equal to the yielding force per unit length F_y/b_n.

NUMERICAL EXAMPLE

Plain Concrete Beam

The first example is due to experimental and numerical results reported by Petersson (1981). It is used here to investigate the Mode I crack propagation by means of a notched beam subjected to three-point bending. The BEM mesh and the boundary condition are shown in Fig. 5(a). In the BEM analysis, the parameters used are beam depth h = 0.2 m, span length l = 2.0 m, width b = 0.05 m, and ratio between initial crack depth and beam depth $a{:}d$ is 0.5. The material properties of the beam are E = 30,000 MPa; f_t' = 3.33 MPa; ν = 0.2, and G_F = 124 N m^{-1}. Both in BEM and FEM analyses, the σ-Δu^{cr} curves are assumed to be SL and BL. In the experimental tests by Petersson (1981), six beams were tested to determine the fracture energy G_F; and it was found that the highest value was 137 N m^{-1}, and the lowest value was 115 N m^{-1}.

The deformed shape at Iterations 4 and 8 are shown Figs. 5(b and c). The load-deflection curves plotted in Fig. 6 show that a good agreement with the FEM analysis and experimental results is obtained. It is observed that the BL of the σ-Δu^{cr} curve gives better results compared to SL both in BEM and FEM analyses.

The second example is a beam tested by Bosco et al. (1990) and has been analyzed using FEM by Hawkins and Hjorteset (1992). In this example a concrete beam (Grade 4) with depth

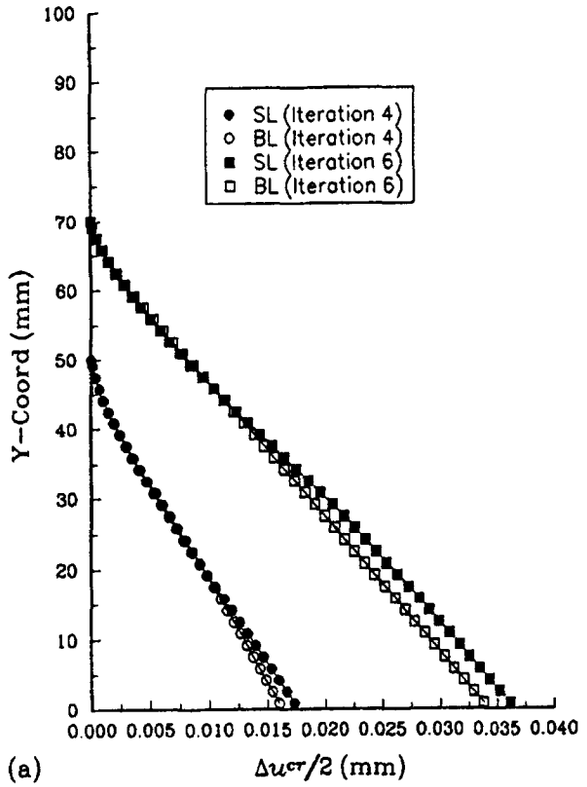

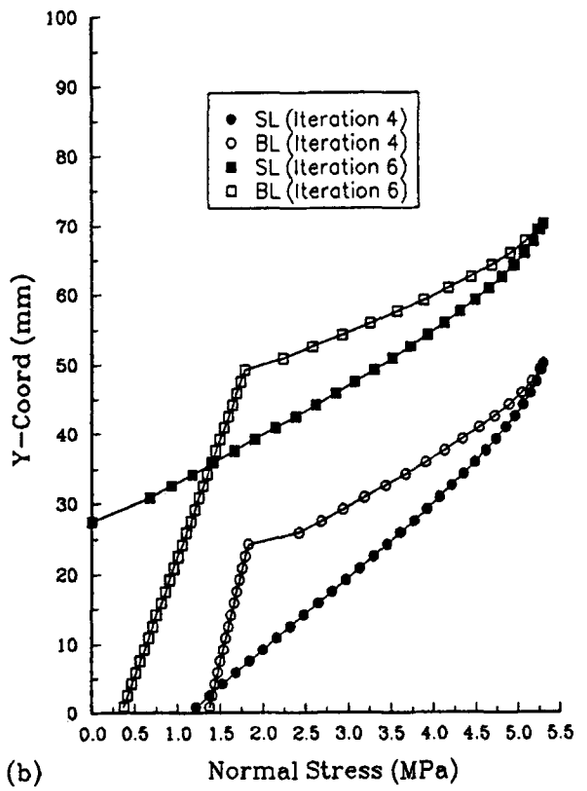

FIG. 9. (a) Crack Opening Displacement; (b) Stresses along Line of Symmetry for Iterations 4 and 6

h = 100 mm, width b = 150 mm, and span l = 600 mm is used. The material properties of the beam are E = 34,300 MPa; f_t' = 5.3 MPa, and ν = 0.2. Fig. 7(a) shows the BEM mesh and its boundary condition. There were 45 elements with 97 nodes in the initial state of the analysis after considering the discontinuous elements on the crack and edge elements that intersect with the crack. The initial crack of 10 mm shown in Fig. 7(a) is not a traction free crack but loaded with the fictitious forces even in the early stage of loading. This was the best configuration to match with the experimental results since BEM analysis needs an initial crack to start the crack growth while in the experimental results it is not essential. The crack extension is chosen as 10 mm and Petersson's BL of σ-Δu^{cr} curve is assumed for the fracture property. The deformed shape at Iterations 4 and 8 is shown in Figs. 7(b) and 6(c), respectively. Fig. 8 shows the load versus midspan deflection by FEM analysis, experimental results, and BEM analysis. The fracture energy G_F used in the FEM analysis was 90 N m^{-1}, and the load-deflection curve indicates that this value is relatively small compared to the load-deflection curve given by the experiment. For this reason, various numbers of G_F in the range of 90–150 N m^{-1} were tested in the BEM analysis, and it was found that higher values of G_F are closer to the experiment.

Fig. 9 shows the crack opening displacement ($\Delta u^{cr}/2$) and stresses along the line of symmetry for Iterations 4 and 6, respectively, for G_F = 90 N m^{-1}. It shows that the crack is completely loaded in Iteration 4 for both SL and BL models, but in Iteration 6, the traction-free crack appear in the SL model and not in the BL model. It is indicated that the prediction of the fracture behavior of concrete is more reliable when using the BL model.

Reinforced-Concrete Beam

The same beam tested by Bosco et al. (1990) is used together with a reinforcement located 10 mm above the bottom surface of the beam. The reinforcement is discretized using 20 elements with 41 nodes of equal intervals. The same number of elements and nodes as in the unreinforced beam is applied for the discretization of the concrete. The area of the reinforcement and the yield stress is varied as shown in Table 1. The crack is assumed to initiate when a value of stress along the bottom surface has reached the maximum tensile stress of concrete f_t'. Fig. 10 shows the stresses along the reinforcement immediately before the crack was initiated. At this stage, the maximum cracking load P_{cr} obtained by BEM analysis is compared with the theoretical analysis of an uncracked section using the triangular stress block by Mosley and Bungey (1987) as shown in Table 1. It can be seen that good agreement is obtained for both results.

The effect of reinforcement over the crack opening displacement can be seen in Fig. 11 for Iterations 4 and 6, respectively, with A_s = 12.7 mm^2. It is clearly shown that the introduction of reinforcement tends to close the crack opening both in SL and BL models.

Fig. 12 shows the load versus mid-span deflection curve obtained by the BEM analysis, FEM analysis, and experimental results for A_s = 12.7 mm^2. The BEM analysis uses various numbers of fracture energy as in the unreinforced beam. The value of G_F = 110 N m^{-1} seems to give good agreement with the experimental result. After the fictitious crack tip crossed the reinforcement, the stresses in the steel stress of 5.8, 8.7, 13.9, 21.2, 31.3, 46.6, and 71.9% of f_y for

TABLE 1. Maximum Cracking Load Immediately before Crack Initiation

h (mm) (1)	b (mm) (2)	Steel (3)	A_s (mm^2) (4)	f_y (MPa) (5)	Cracking Load P_{cr} (kN)		
					BEM (6)	Theory (7)	Percentage (8)
100	150	1ϕ4	12.7	637	9.05	8.95	−1.10
100	150	2ϕ5	39.3	569	9.30	9.21	−0.97
100	150	2ϕ8	100.5	441	9.88	9.79	−0.91
100	150	2ϕ10	157.1	456	10.41	10.32	−0.86

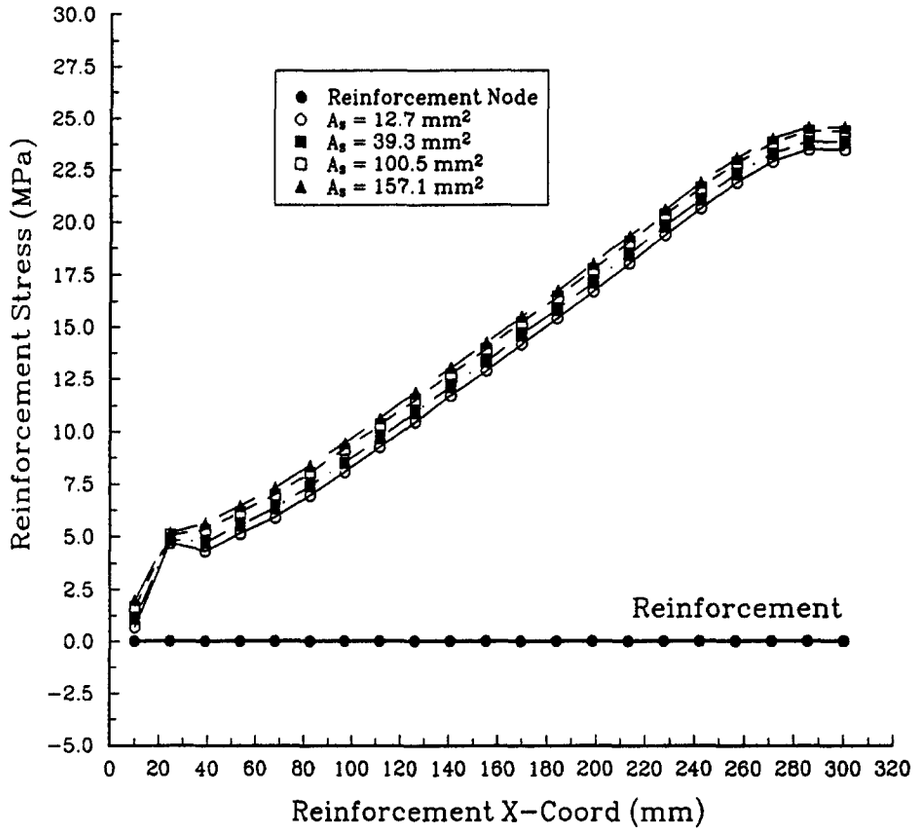

FIG. 10. Stresses along Reinforcement Immediately before Crack Initiation for Different A_s Values

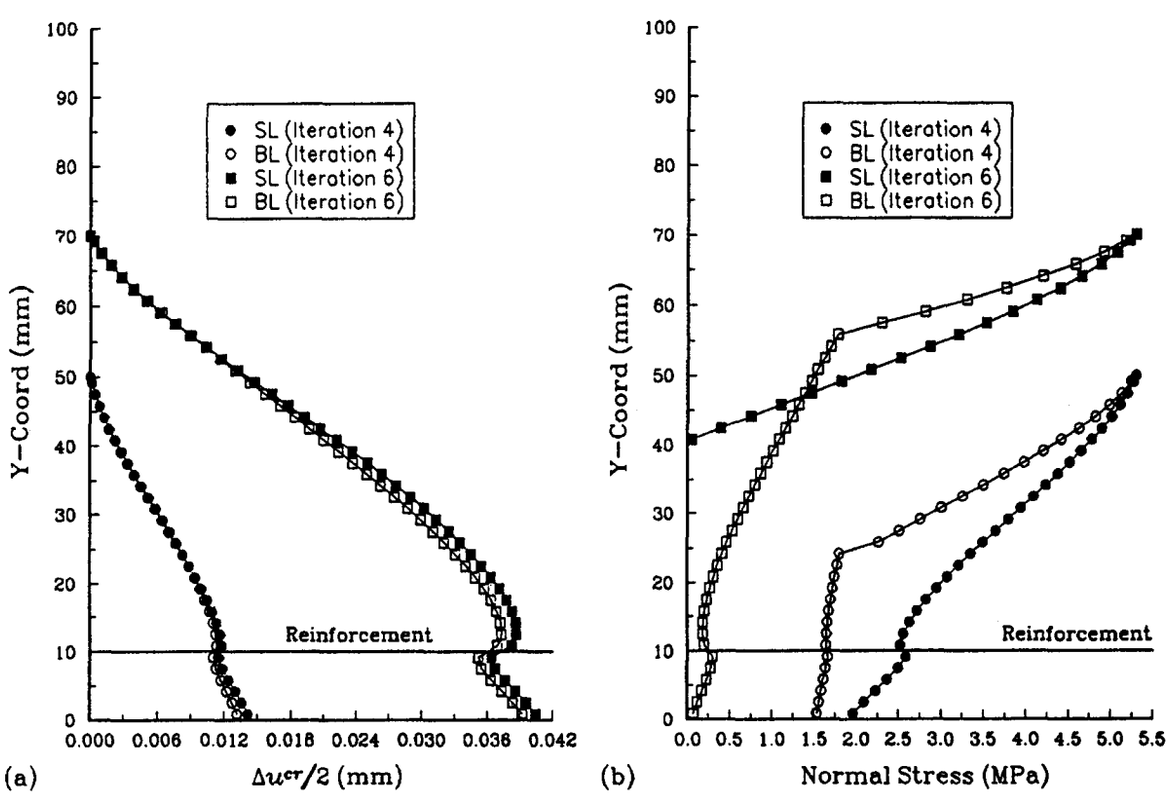

FIG. 11. (a) Crack Opening Displacement; (b) Stresses along Line of Symmetry for Iterations 4 and 6 in Reinforced Concrete

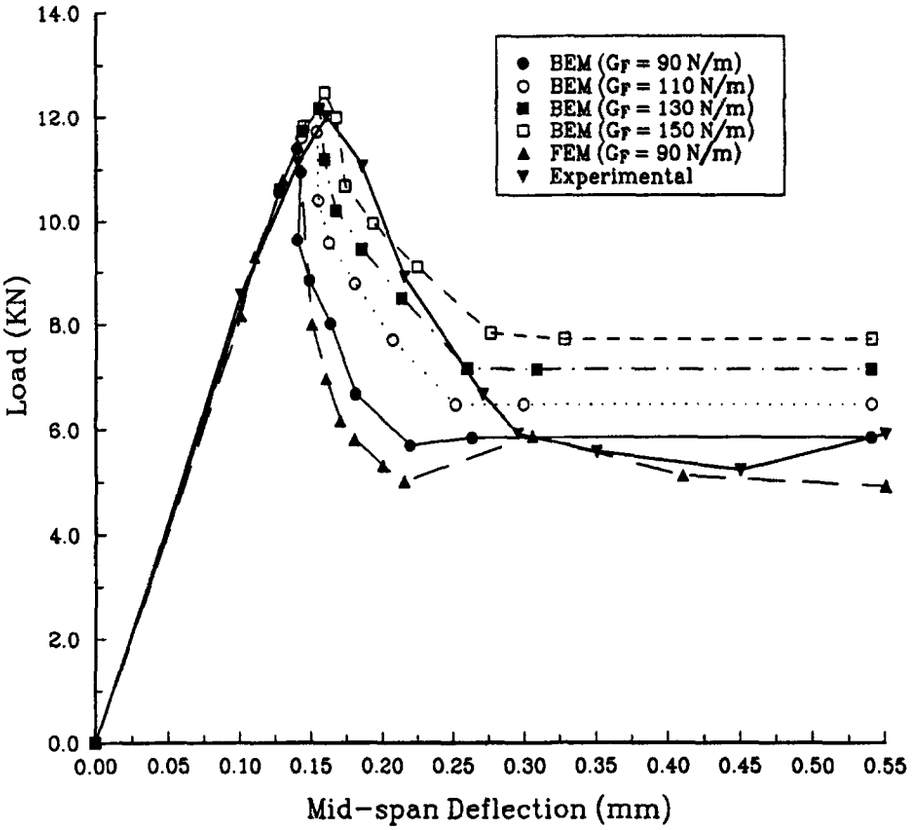

FIG. 12. Load-Deflection Curves for Reinforced-Concrete Beam with Various G_F: BEM Analysis, FEM Analysis, and Experimental Results

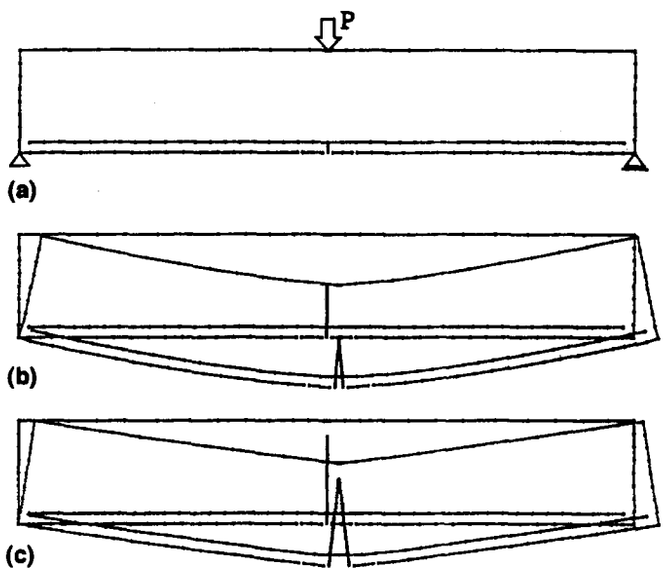

FIG. 13. (a) Boundary-Element Mesh; Deformed Shape for: (b) Iteration 4; (c) Iteration 8 with Reinforcement

fictitious crack tip located at 20, 30, 40, 50, 60, 70, and 80 mm were observed. Note that the steel stresses increase markedly only after the traction-free crack has developed (i.e., when the fictitious crack tip reaches a depth of 80 mm).

The steel yielding was observed when the fictitious crack tip approached a depth of 90 mm. At this stage the load was kept constant until the strain in the steel exceeded the ultimate capacity ε_u as shown in Fig. 12. The initial BEM mesh and the deformed shape in Iterations 4 and 8 are shown in Fig. 13.

Fig. 14 shows the load-deflection curve for the various reinforcement areas. In all cases the value of G_F is taken as 110 N m^{-1}.

The load-deflection curve obtained by BEM analysis are not in good agreement with the experimental result by Carpinteri (1990) due to the assumption of a perfect bond and the unrealistic assumption of cracking on the center line only. The predicted maximum load capacities are however, reasonably accurate for all cases.

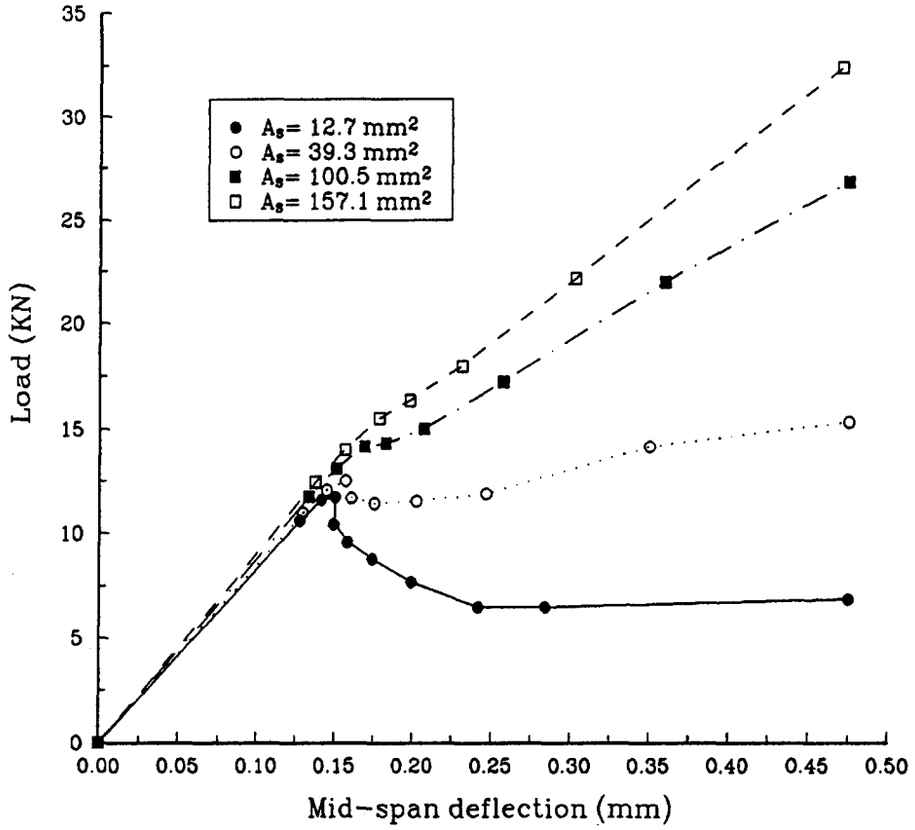

FIG. 14. Load-Deflection Curves for Reinforced-Concrete Beam with Different A_s Values

CONCLUSIONS

A boundary-element formulation has been presented for modeling cracking in plain and reinforced concrete. The model utilized the FCM for the cracking of concrete. Both the linear and bilinear stress-displacement curve have been implemented. The BEM results were shown to agree well with the FEM and experimental results. The advantage of the new formulation over previous ones was demonstrated by simulating crack growth where no remeshing is required.

The embedded approach is used to model the reinforcement. The proposed model has a capability to detect the yield stress in the steel with reasonable accuracy. It is assumed that the bond between steel and concrete is perfect; however, modification can be made to include bond slip by setting the value of $\Phi'' \neq 0$.

The BEM results for the maximum cracking load of the reinforced-concrete beam are in excellent agreement with the theoretical results. As expected the results show that the introduction of reinforcement slows the grack growth rates.

APPENDIX. REFERENCES

Bosco, C., Carpinteri, A., and Debernardi, P. G. (1990). "Minimum reinforcement in high-strength concrete." *J. Struct. Engrg.*, ASCE, 116, 427–437.

Hawkins, N. M., and Hjorteset, K. (1992). "Minimum reinforcement requirements for concrete flexural members." *Applications of fract. mech. to reinforced concrete*, A. Carpinteri, ed., Chap 15, Elsevier Applied Science, London, England, 379–412.

Mosley, W. H., and Bungey, J. H. (1987). *Reinforced concrete design.* MacMillan Education Ltd., London, England.

Petersson, P. E. (1981). "Crack growth and development of fracture zones in plain concrete and similar materials." *Rep. No. TVBM-1006*, Div. of Build. Mat., Lund Inst. of Technol., Lund, Sweden.

Saleh, A. L., and Aliabadi, M. H. (1995). "Crack growth analysis in concrete using boundary element method." *Engrg. Fract. Mech.*, 51(4), 533–545.

Salgado, N. K., and Aliabadi, M. H. (1994). "Boundary element analysis of cracked stiffened panels." *Proc., Boundary Element Method XVI*, C. A. Brebbia, ed., Computational Mechanics Publications, Southampton, U.K., 477–484.